Multi-GNSS Tomography: Case Study of the July 2021 Flood in Germany

Karina Wilgan, Hugues Brenot, Riccardo Biondi, Galina Dick, and Jens Wickert

Abstract

Due to climate change, intensive storms and severe precipitation will continue to happen, causing destructive flooding. In July 2021, a series of storms with prolonged rain episodes took place in Europe. Several countries were affected by severe floods following that rainfall, causing many deaths and material damage. Thus, a good understanding and forecasting of such events are of uttermost importance. This study highlights the interest of multi-GNSS tomography for the 3D modelling of the neutral atmosphere refractivity. The tropospheric parameters have been retrieved for the July 2021 flood in Germany from two tomographic solutions with different constraining options using either GPS-only or multi-GNSS estimates. Our investigations show that the stand-alone solution (especially the multi-GNSS) is producing more patterns of refractivity, and is temporally more stable. We compare the tomographic results with external observations such as radiosondes and GNSS radio-occultations from Metop-A & -B satellites. The results show that tomography is producing wetter conditions than the reference. However, we can see the precursor information of the initiation of deep convection in the ground-based GNSS technique.

Keywords

Deep convection · GNSS tomography · Multi-GNSS · Severe weather events

1 Introduction

GNSS tomography is a technique that unwraps a simple integrated signal into a 3D distribution of the atmosphere parameters, usually related to water vapor (Flores et al. 2000; Seko et al. 2000; Gradinarsky and Jarlemark 2004; Champollion et al. 2005). The method is based on the inverse Radon transform (Fiddy 1985), which states that a continuous field can be successfully reconstructed from integrated observations providing an infinite number of observations penetrating the field from an infinite number of angles. Due to the geometrical constraints such as one-way communication between satellite and receiver, availability of visible satellites only above the receiver, and very limited number of side observations, the tomography system is ill-conditioned and ill-posed (Troller et al. 2006), which evokes many research questions.

The idea of GNSS tomography originated in the early 2000s (Flores et al. 2000). In the traditional voxel approach, the tropospheric parameters, i.e. the refractivity or water vapor density, are obtained from the GNSS Slant Tropospheric Delay (STD) products on a 3D grid (voxels). Many methodological enhancements have been introduced. Some

K. Wilgan (✉) · J. Wickert
Technische Universität Berlin (TUB), Berlin, Germany

German Research Centre for Geosciences (GFZ), Potsdam, Germany
e-mail: karina.wilgan@gfz-potsdam.de

H. Brenot
Royal Belgian Institute for Space Aeronomy (BIRA-IASB), Brussels, Belgium

R. Biondi
University of Padova, Padova, Italy

G. Dick
German Research Centre for Geosciences (GFZ), Potsdam, Germany

included adding supplementary data from external sources into the functional model (e.g., Bender et al. 2011a; Rohm et al. 2014), some new parametrizations (e.g., Perler et al. 2011; Brenot et al. 2019). Improvements are expected by using multi-GNSS (Bender et al. 2011b). The recent studies focus on function-based tomography, instead of voxel-based (e.g., Haji-Aghajany et al. 2020; Forootan et al. 2021).

In this study, we focus on the voxel-based tomography using multi-GNSS STD retrievals for a part of Germany that was affected by severe rainfall and flooding in July 2021. We have retrieved the total refractivity using Singular Value Decomposition method, with a novel iterative approach. We show the comparisons of the tomography-based total refractivity from different strategies with the reference data.

2 Data and Meteorological Conditions

We retrieve the tomography solutions for the period of July 10–18, when the severe rainfall and devastating floods in Europe occurred. The rain episodes started between July 6 and 12. Additional heavy precipitation on July 13–15 along with the slow-moving pressure system led to destructive flooding (Puca et al. 2021). In Germany, the most affected regions were North Rhine-Westphalia and Rhineland-Palatinate, especially in the district of Ahrweiler. In Cologne, the rain gauges indicated 154 mm of rainfall for July 14, the day of the highest rainfall. More detail on the meteorological conditions can be found in Wilgan et al. (2023). Figure 1

shows the chosen tomography area, indicating the GNSS stations and their GPS (G), GLONASS (R) and Galileo (E) signals' capability. The GNSS data are calculated using the GFZ-developed software EPOS.P8 with 2.5 min temporal resolution for the 70 stations located between 6° and 10° longitude and 49° and 52° latitude. More details about the processing can be found in Wilgan et al. (2022).

Figure 1 also shows the location of the radiosonde (RS) station Essen, 10410 (near GNSS station EDZE), situated within the tomography region as well as the two radio-occultations (RO) from Metop-A&B satellites that occurred during our chosen period (July 15, 19:55 UTC and July 14, 17:07 UTC). Both RS and RO are used as reference data in this study. The GNSS RO can be used to retrieve the vertical properties of the atmosphere with high accuracy and high vertical resolution (Scherllin-Pirscher et al. 2011). Each GPS Receiver for Atmospheric Sounding (GRAS) on board of the Metop satellites (Luntama et al. 2008) provides more than 600 daily atmospheric profiles globally distributed and it is the only operational RO instrument at the moment. The ROs can be downloaded here: https://www.cosmic.ucar.edu/what-we-do/data-processing-center/data.

The a priori model for tomography and another reference is Numerical Weather Model (NWM) Icosahedral Nonhydrostatic (ICON) run by the German Weather Service (DWD). We have used the nested ICON-D2 version of the global model with the resolution of 0.02° × 0.02° with 65 vertical layers up to 20 km. The GNSS ZTDs and ROs are assimilated into the ICON global model, but not into the nested, regional model.

Fig. 1 The location of the tomography region with marked GNSS and radiosonde stations as well as the two radio-occultations
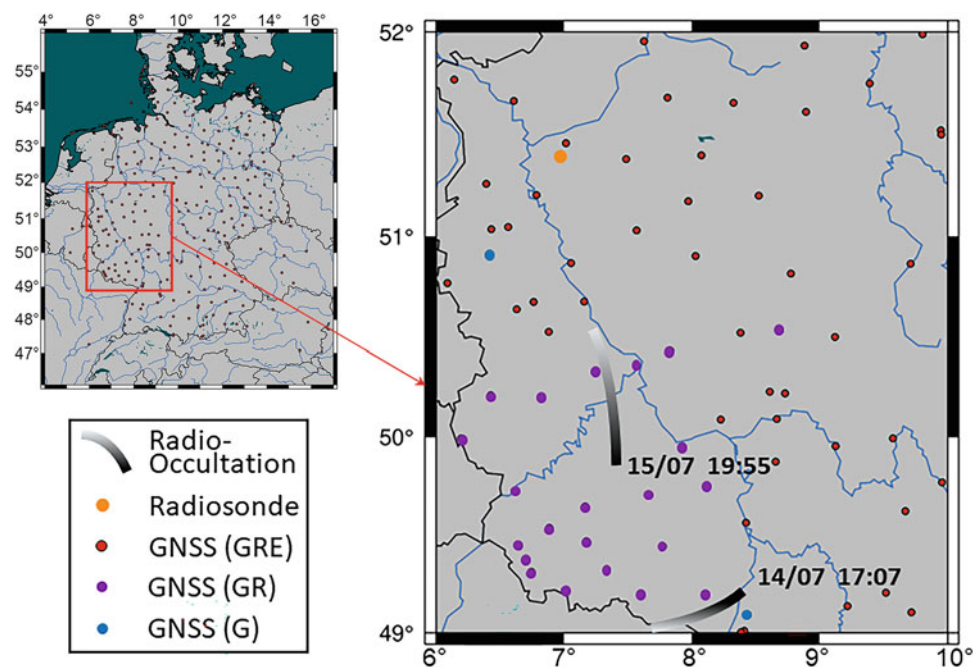
3 Strategy of GNSS Tomography

Located in western Germany (see Fig. 1), the tomography grid has a latitude × longitude horizontal resolution of $0.2° × 0.3°$ ($21 × 22$ km^2; $15 × 14$ elements). With 15 vertical levels, from 0 km above the sea level, every km until 15 km, the number of tomography voxels is 3,150. The temporal resolution of tomography matches the 2.5 min resolution of the GNSS data. We retrieve the total refractivity with the GNSS tomography principle, i.e., using the GNSS STDs. The STD can be related to the total refractivity N_{tot} using the equation:

$$STD = 10^{-6} \int N_{tot} ds \cong 10^{-6} \sum N_{tot} \Delta s. \quad (1)$$

The tomographic model m can be represented as:

$$m = m_0 + \left(G^t C_d^{-1} G + C_m^{-1}\right)^{-1} G^t C_d^{-1} (d - Gm_0), \quad (2)$$

where d is the data (GNSS STDs), G the geometrical matrix ($15 × 14 × 15$ voxels), m the model solution (calculated using Singular Value Decomposition), m_0 a priori model (forecasts from the ICON-D2), C_d the covariance operator of the data and C_m covariance operator of the a priori model.

The solutions are calculated using an iteration process, which stops when the absolute bias between previous and new retrievals is under 1% (convergence to the final solution). C_d characterizes the confidence in the data and C_m the confidence in the a priori model. In this study, we test estimates of $C_d = (STD * coeff\_C_d)^2$ with $coeff\_C_d = 10\%$, 15%, 20%, 25% or 30%, and $C_m = (N_{ap} *coeff\_Cm)^2$ with $coeff\_Cm = 90\%$, 85%, 80%, 75% or 70%. N_{ap} is the refractivity from the m_0 a priori model. The interest of using multi-GNSS in tomography is to improve the geometrical representation by increasing the number of forced voxels (the ones that tomography retrieves, i.e., with STDs crossing the voxels). In this study, for the G solution, the number of forced voxels is 70% (2,205 voxels) and it is improved to 74% (2,331 voxels) and 76% (2,394 voxels) by using GR and GRE, respectively.

We have used two types of tomographic solutions: constrained and stand-alone. In the constrained solution, we take the hourly a priori information from the ICON-D2, while in the stand-alone solution, ICON-D2 is used only to initiate the tomography, and then a priori values are taken from the previous tomography retrievals (TRs). On average, three iterations are needed for the constrained solution and only one iteration is required for the stand-alone solution.

4 Results

This section shows the results of the tomography retrievals. First, we compare different solutions with each other and then the TRs to the reference ICON-D2, RS and RO data.

4.1 Tomography Cross-Section

We present the total refractivity values obtained using the constrained and stand-alone solutions. Figure 2 shows the results using different GNSS signals: G, GR and GRE for a sample date and height of 1.5 km and Fig. 3 the time evolution of the two TRs for a fixed altitude and longitude.

We can see in Fig. 2 that the three constrained solutions are similar, while the three stand-alone solutions show stronger differences with more patterns. Especially the GRE solution shows more variability, compared to the G and GR solutions, which are closer to each other. However, if we have considered solutions for the consecutive times (Fig. 3), we can see that the constrained solutions show a lot more time variability as they try to move from the a priori ICON-D2 to the converge solution (closer to the stand-alone results), while the stand-alone solutions are smoother. In the above comparisons, a set-up of $coeff\_C_d = 10\%$ and $coeff\_C_m = 90\%$ is used. These parameters indicate how much confidence we have in the data and the a priori model, respectively, and can be modified. Figure 4 shows five different set-ups of the covariance parameters for the GRE stand-alone solutions. We can see that the set-ups differ from each other. The higher the $coeff\_C_d$ values, the lower the refractivity obtained with this solution. More detailed analyses are in the comparisons with RS and RO chapters.

4.2 Comparisons with ICON-D2

In the next step, we compare the TRs to the reference ICON-D2 data. Please note that these comparisons are not independent, because ICON data is used as a priori to calculate the tomography solutions. Figure 5 shows the total refractivity fields from ICON and TRs for the GRE solution on 13 July 2021, at 08:00 UTC and for the altitude of 1.5 and 2.5 km. For the constrained solution, the Root-Mean-Square Error (RMSE) is 11.4 ppm (12.5 ppm for the ICON datasets from July 10–18, 2021), and 15.7 ppm (17.9 ppm) for the stand-alone solution.
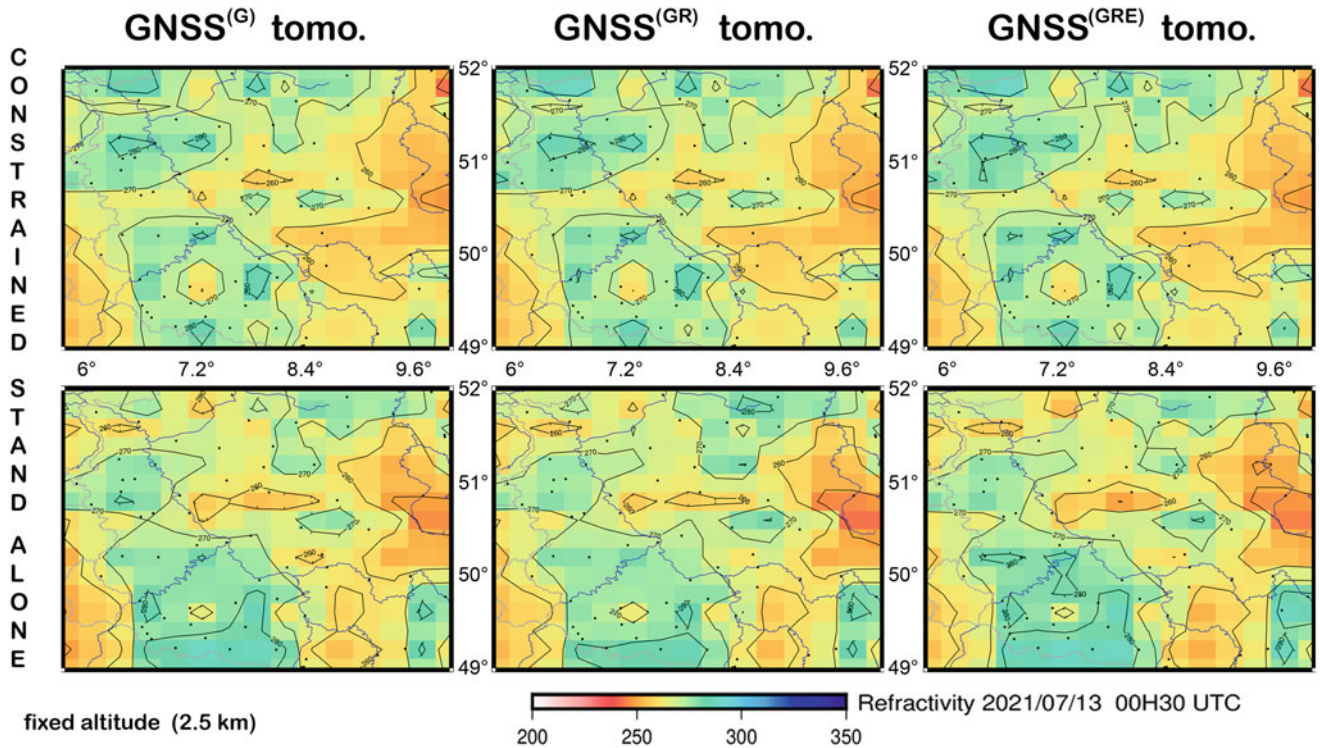
Fig. 2 Total refractivity from the constrained (top) and stand-alone (bottom) TR (G, GR and GRE solutions, from left to right) on 13 July, 00:30 UTC, for a fixed altitude of 2.5 km a.s.l.
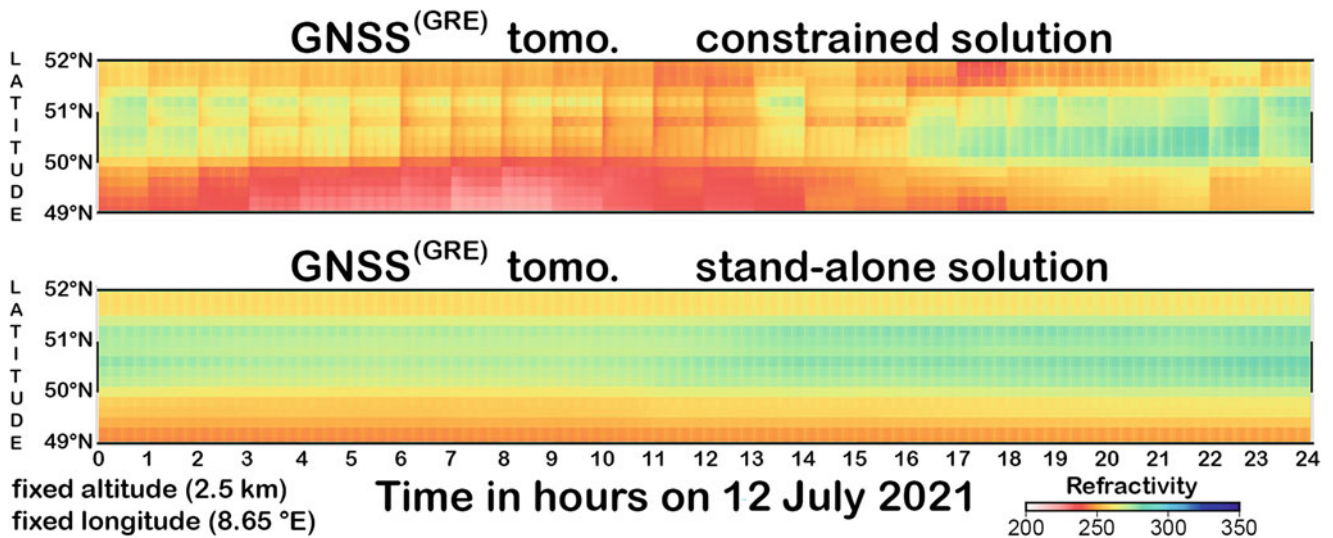

Fig. 3 Total refractivity from the constrained (top) and stand-alone (bottom) TR (GRE solution) on 12 July, from 00:00 to 24:00 UTC, for a fixed altitude (2.5 km) and a fixed longitude (8.65°E)

As shown in Fig. 5, the TRs are producing wetter conditions than ICON data. Moreover, the constrained solution is 40% closer to ICON than the stand-alone, which is not surprising, as we have used ICON as the a priori for the constrained solution. However, the two TRs are still closer to each other than to ICON, with a RMSE of 8.4 ppm (10.2 ppm) for the G solutions, and 6.3 ppm (8.0 ppm) for the GRE solutions. Moreover, closer to the ground (1.5 km vs 2.5 km) and when deep convection took place on July 13 northeastwards of the Grand Duchy of Luxembourg, Fig. 5 shows more structured refractivity fields, as there, the water vapor content and thus refractivity is higher and more variable. Such pattern is not seen by ICON, even though it offers more detailed fields, as the resolution of the model is 0.02°, which is 10 times larger than TRs.
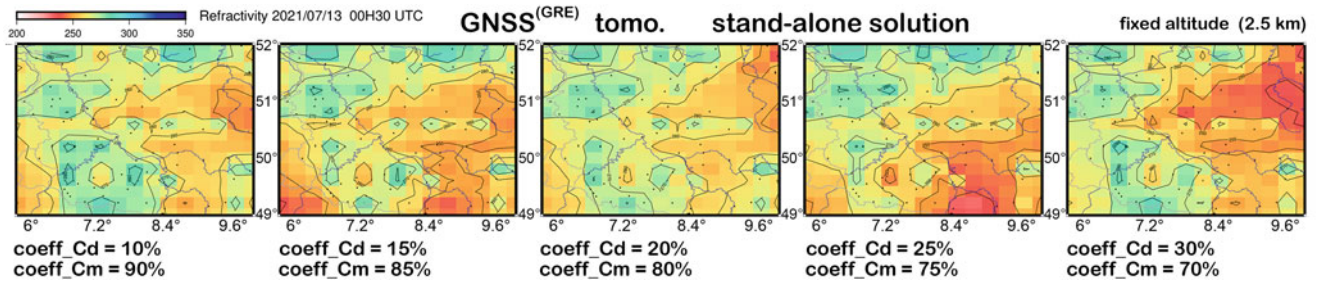
Fig. 4 The evaluation of using different covariance values coeff_C_d = 10%, 15%, 20%, 25%, 30% while coeff_C_m = 90%, 85%, 80%, 75%, 70%. Results are shown for the stand-alone GRE TR
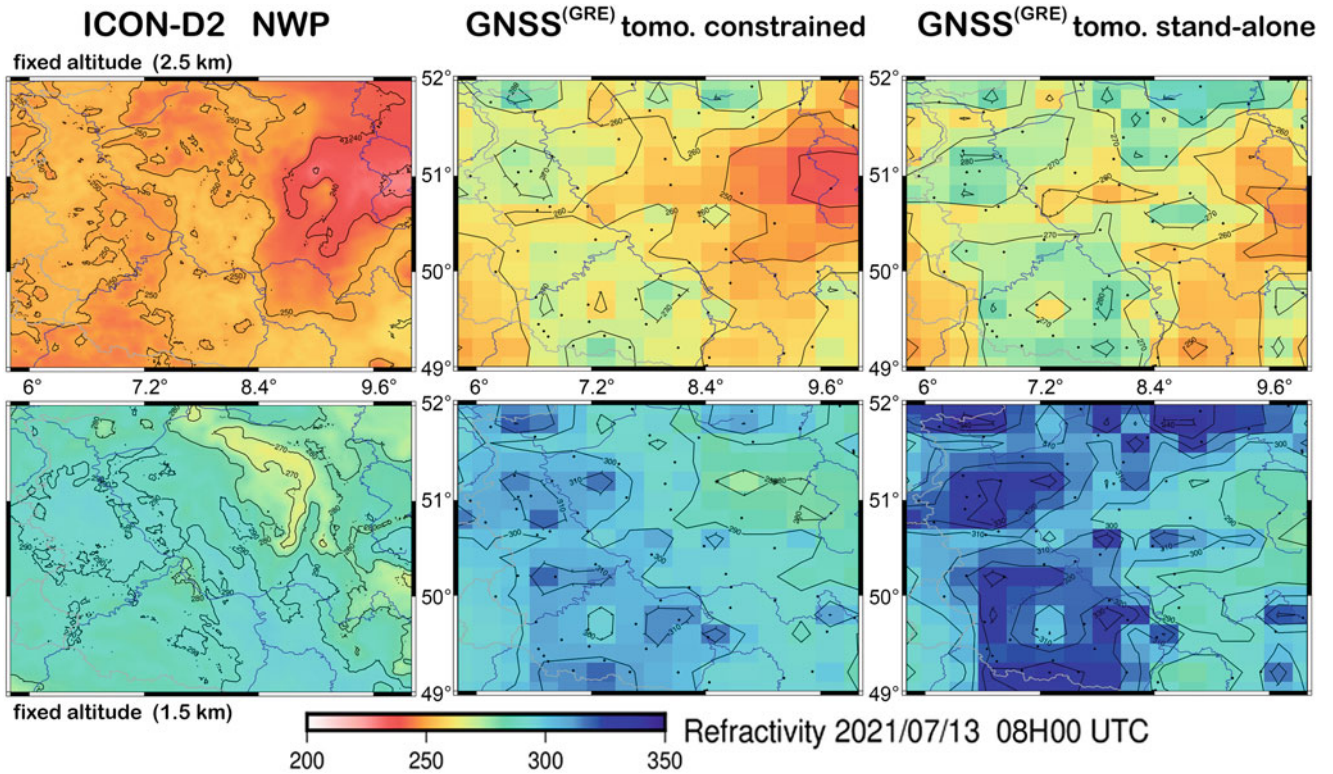
Fig. 5 Comparison of ICON (left), GRE tomography constrained (middle) and GRE tomography stand-alone (right) for July 13 (08:00 UTC), height 2.5 km (top) and 1.5 km (bottom)

### 4.3 Comparisons with Radiosonde Data

Another reference data in this study is radiosonde. There is one RS station 10410 located in the north-east of the chosen area, in Essen (see Fig. 1). Figure 6 shows the total refractivity values from the RS, ICON and TR from G and GRE solutions for a sample date of July 13, 0:00 UTC. The RMSE RS-ICON is of 5.2 ppm (4.3 ppm for the 18 radiosondes from July 10–18, 2021).

As seen in Fig. 6, RS and ICON data are closer to each other than to the TRs, meaning that tomography produces wetter conditions than the reference data. For the constrained retrievals, both G and GRE solutions are very similar (RMSE of 1.2 ppm for the 18 radiosondes), but, there are some differences for the stand-alone solution (RMSE of 4.7 ppm), where

GRE is closer to the reference data (RMSE of 15.7 ppm against 17.3 ppm for the G solution). In the bottom panel, we see the impact of using different covariance operators for the stand-alone GRE solution. The variant with $coeff\_C_d = 20\%$ and $coeff\_C_m = 80\%$ is closer to the RS on the ground level (15% decrease of the RMSE with respect to the solution with $coeff\_C_d = 10\%$ and $coeff\_C_m = 90\%$), while with $coeff\_C_d = 30\%$ and $coeff\_C_m = 70\%$ is the closest for the middle layers (45% decrease of the RMSE).

4.4 Comparisons with Radio-Occultations

In the next step, the TRs are compared to the RO data (two profiles; see Fig. 1). Figure 7 shows the total refractivity
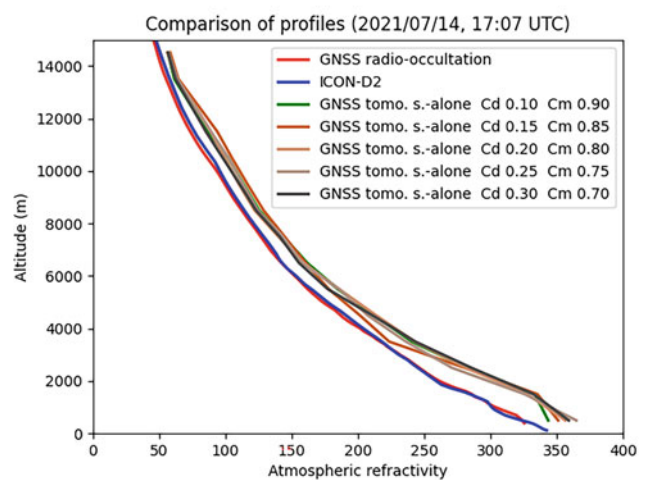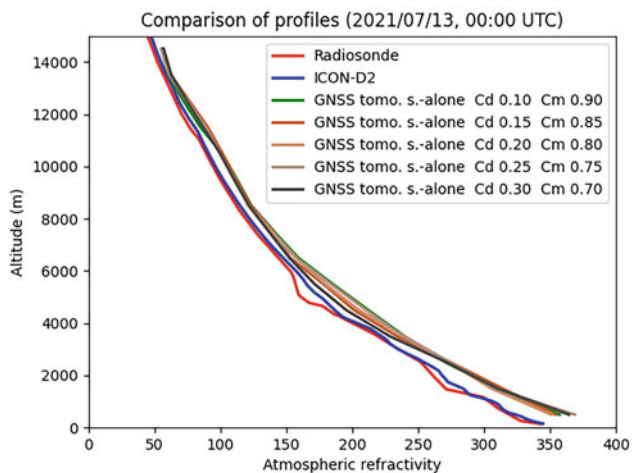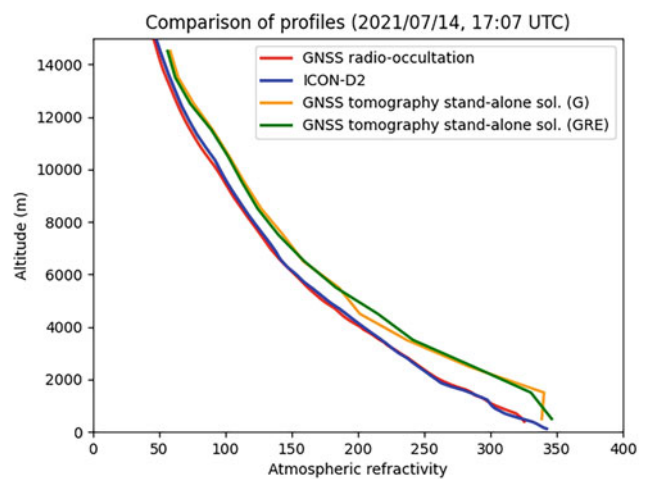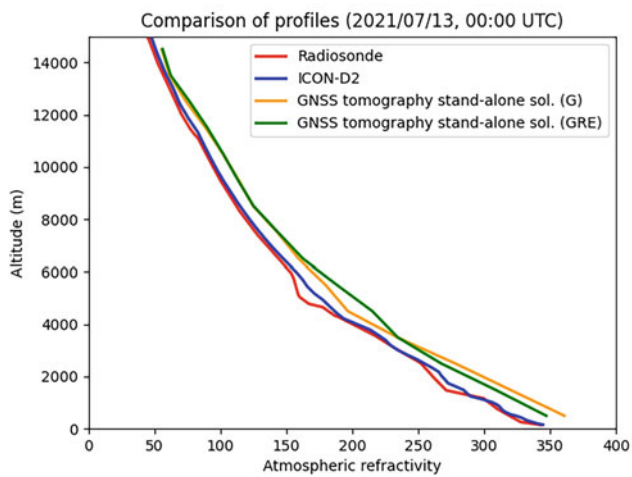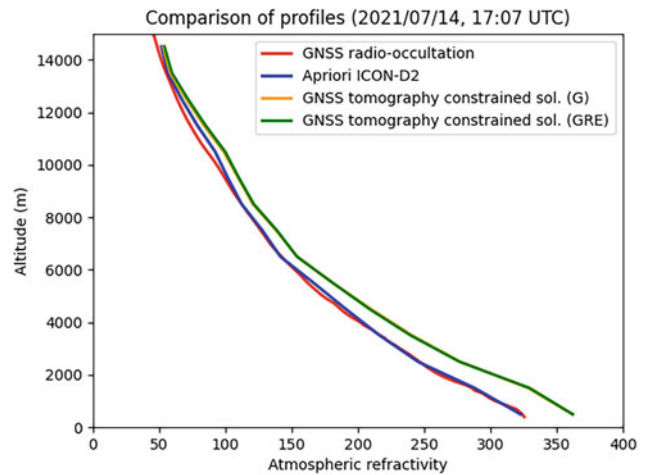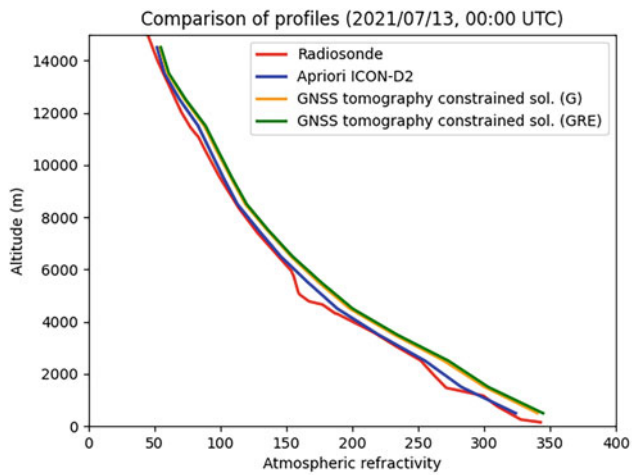
Fig. 6 Reference RS and ICON-D2 data vs. TRs for the constrained (top), stand-alone (middle) and stand-alone solution with different covariance operators (bottom) solutions

Fig. 7 Reference RO and ICON-D2 data vs. TRs for the constrained (top), stand-alone (middle) and stand-alone solution with different covariance operators (bottom) solutions

from RO, ICON and TRs for July 14, 17:07, one of the occultations occurrences.

As shown in Fig. 7, for the RO we have a similar situation to RS: the RO and ICON are close to each other (RMSE of 3.1 ppm for the two ROs), while the TRs are producing wetter conditions (RMSE of about 21 ppm for the G/GRE constrained/stand-alone solutions). Here, we see an improvement for the stand-alone GRE solution for the layer close to the ground, i.e., under 3 km with a 28% decrease of the RMSE, however, a 25% increase of the RMSE is observed for the middle layers, i.e., between 4 and 8 km. From the covariance parameters, the closest to RO is $coeff\_C_d = 10\%$ and $coeff\_C_m = 90\%$ for the lowest layers and $coeff\_C_d = 15\%$ and $coeff\_C_m = 85\%$ for the middle layers (26% decrease of the RMSE with respect to the solution with $coeff\_C_d = 10\%$ and $coeff\_C_m = 90\%$), so slightly different options than for RS.

5 Conclusions

We showed the first results of multi-GNSS tomography for a severe precipitation and flooding event in July 2021. We presented a new retrieval algorithm with an iteration process for stand-alone and constrained tomography solutions based on G, GR and GRE data. The two types of TRs differed between each other, especially in space, where the stand-alone solution was smoother, while the constrained solution tried to converge to the a priori data, here taken from ICON. The GRE solution was the best fit, as it showed more patterns in the obtained total refractivity. Using the multi-GNSS also retrieved more forced voxels. The TRs were compared with reference ICON, RS and RO data. In general, the TRs tended to produce wetter conditions compared to the reference data, which was, however, in line with the previous findings. During the phase of the initiation of deep convection on July 13, 2021, TRs show high values of total refractivity northeastwards of the Grand Duchy of Luxembourg (see Fig. 5), which is not seen by ICON-D2 NWM and could be substantial information to be considered in an assimilation system.

Moreover, we checked the impact of different covariance operators on the tomography retrievals. We reached a better agreement with the reference data for some of the variants. TRs show wetter estimates for the lower layers (between 0 and 3 km) than reference external solutions. As the impact of GNSS ground-based data is stronger for the lower layers than for the middle layers (between 3 and 5 km), we suggest using a low covariance coefficient for the data ($coeff\_C_d = 10\%$) and a high covariance coefficient for the a priori model ($coeff\_C_m = 90\%$). However, this requires having good a priori estimates. To improve the quality of TRs, we think a mixed strategy/solution can be implemented, which combines the use of conservative covariance for the lower layers and less conservative coefficients for the middle layers (e.g., with $coeff\_C_d = 20\%$ and $coeff\_C_m = 80\%$).

References

Bender M, Dick G, Ge M, Deng Z, Wickert J, Kahle HG, Raabe A, Tetzla G (2011a) Development of a GNSS water vapour tomography system using algebraic reconstruction techniques. Adv Space Res 47:1704–1720

Bender M, Stosius R, Zus F, Dick G, Wickert J, Raabe A (2011b) GNSS water vapour tomography—expected improvements by combining GPS, GLONASS and Galileo observations. Adv Space Res 47(5):886–897

Brenot H, Rohm W, Kačmařík M, Möller G, Sá A, Tondaś D et al (2019) Cross-comparison and methodological improvement in GPS tomography. Remote Sens 12(1):30

Champollion C, Masson F, Bouin MN, Walpersdorf A, Doerflinger E, Bock O, Van Baelen J (2005) GPS water vapour tomography: preliminary results from the ESCOMPTE field experiment. Atmos Res 74(1-4):253–274

Fiddy MA (1985) The radon transform and some of its applications. Opt Acta 32(1):3–4

Flores A, Rufifni G, Rius A (2000) 4D tropospheric tomography using GPS slant wet delays. Ann Geophys 18:223–234

Forootan E, Masood D, Saeed F, Ali SK (2021) A functional modelling approach for reconstructing 3 and 4 dimensional wet refractivity fields in the lower atmosphere using GNSS measurements. Adv Space Res 68(10):4024–4038

Gradinarsky L, Jarlemark P (2004) Ground-based GPS tomography of water vapor: analysis of simulated and real data. J Meteorol Soc Jpn 82(1B):551–560

Haji-Aghajany S, Amerian Y, Verhagen S (2020) B-spline function-based approach for GPS tropospheric tomography. GPS Solut 24(3):88

Luntama JP, Kirchengast G, Borsche M, Foelsche U, Steiner A, Healy S, von Engeln A, O'Clerigh E, Marquardt C (2008) Prospects of the EPS GRAS mission for operational atmospheric applications. Bull Am Meteorol Soc 89(12):1863–1875

Perler D, Geiger A, Hurter F (2011) 4D GPS water vapor tomography: new parameterized approaches. J Geod 85:539–550

Puca S, Brocca L, Panegrossi G et al (2021) A slow moving upper-level low brought devastating floods to parts of north west Germany and other parts of western Europe in July 2021. https://www.eumetsat.int/devastating-floods-western-europe. Published 26.07.2021

Rohm W, Zhang K, Bosy J (2014) Limited constraint, robust Kalman filtering for GNSS troposphere tomography. Atmos Meas Tech 7(5):1475–1486

Scherllin-Pirscher B, Steiner AK, Kirchengast G, Kuo YH, Foelsche U (2011) Empirical analysis and modeling of errors of atmospheric profiles from GPS radio occultation. Atmos Meas Tech 4(9):1875–1890

Seko H, Shimada S, Nakamura H, Kato T (2000) Three-dimensional distribution of water vapor estimated from tropospheric delay of GPS data in a mesoscale precipitation system of the Baiu front. Earth Planets Space 52:927–933

Troller M, Geiger A, Brockmann E, Bettems JM, Bürki B, Kahle HG (2006) Tomographic determination of the spatial distribution of water vapor using GPS observations. Adv Space Res 37(12):2211–2217

Wilgan K, Dick G, Zus F, Wickert J (2022) Towards operational multi-GNSS tropospheric products at GFZ Potsdam. Atmos Meas Tech 15(1):21–39

Wilgan K, Dick G, Zus F, Wickert J (2023) Tropospheric parameters from multi-GNSS and numerical weather models: case study of severe precipitation and flooding in Germany in July 2021. GPS Solut 27(1):1–17